Spectral response of an upconversion detector and spectrometer

Paulina S. Kuo,[1,2,*] **Oliver Slattery,**[1] **Yong-Su Kim,**[1] **Jason S. Pelc,**[3]
M. M. Fejer,[3] **and Xiao Tang**[1]

[1]*Information Technology Laboratory, National Institute of Standards and Technology, Gaithersburg, Maryland 20899, USA*
[2]*Joint Quantum Institute, National Institute of Standards and Technology & University of Maryland, Gaithersburg, Maryland 20899, USA*
[3]*E. L. Ginzton Laboratory, Stanford University, Stanford, California 94305, USA*
[*]*paulina.kuo@nist.gov*

Abstract: We investigate the spectral response of an upconversion detector theoretically and experimentally, and discuss implications for its use as an infrared spectrometer. Upconversion detection is based on high-conversion-efficiency, sum-frequency generation (SFG). The spectral selectivity of an upconversion spectrometer is determined by the SFG spectral response function. This function changes with varying pump power. Working at maximum internal conversion efficiency is desirable for high sensitivity of the system, but the spectral response function is different at this pump power compared to the response function at low power. We calculate the theoretical spectral response of the upconversion detector as a function of pump power and obtain excellent agreement with upconversion spectra measured in a periodically poled $LiNbO_3$ waveguide.

References and links

1. A. P. Vandevender and P. G. Kwiat, "High efficiency single photon detection via frequency upconversion," J. Mod. Opt. **51**, 1433–1445 (2004).
2. C. Langrock, E. Diamanti, R. V. Roussev, Y. Yamamoto, M. M. Fejer, and H. Takesue, "Highly efficient single-photon detection at communication wavelengths by use of upconversion in reverse-proton-exchanged periodically poled $LiNbO_3$ waveguides," Opt. Lett. **30**, 1725–1727 (2005).
3. L. Ma, O. Slattery, and X. Tang, "Single photon frequency up-conversion and its applications," Phys. Rep. **521**, 69–94 (2012).
4. Q. Zhang, C. Langrock, M. M. Fejer, and Y. Yamamoto, "Waveguide-based single-pixel up-conversion infrared spectrometer," Opt. Express **16**, 19557–19561 (2008).
5. L. Ma, O. Slattery, and X. Tang, "Experimental study of high sensitivity infrared spectrometer with waveguide-based upconversion detector[1]," Opt. Express **17**, 14395–14404 (2009).
6. M. D. Eisaman, J. Fan, A. Migdall, and S. V. Polyakov, "Invited review article: Single-photon sources and detectors," Rev. Sci. Instrum. **82**, 071101 (20011).
7. A. Restelli, J. C. Bienfang, and A. L. Migdall, "Single-photon detection efficiency up to 50% at 1310 nm with an InGaAs/InP avalanche diode gated at 1.25 GHz," Appl. Phys. Lett. **102**, 141104 (2013).
8. A. E. Lita, A. J. Miller, and S. W. Nam, "Counting near-infrared single-photons with 95% efficiency," Opt. Express **16**, 3032–3040 (2008).
9. J. S. Pelc, L. Ma, C. R. Phillips, Q. Zhang, C. Langrock, O. Slattery, X. Tang, and M. M. Fejer, "Long-wavelength-pumped upconversion single-photon detector at 1550 nm: performance and noise analysis," Opt. Express **19**, 21445–21456 (2011).

10. G.-L. Shentu, J. S. Pelc, X.-D. Wang, Q.-C. Sun, M.-Y. Zheng, M. M. Fejer, Q. Zhang, and J.-W. Pan, "Ultralow noise up-conversion detector and spectrometer for the telecom band," Opt. Express **21**, 13986–13991 (2013).
11. P. S. Kuo, J. S. Pelc, O. Slattery, Y.-S. Kim, M. M. Fejer, and X. Tang, "Reducing noise in single-photon-level frequency conversion," Opt. Lett. **38**, 1310–1312 (2013).
12. Y. R. Shen, *The Principles of Nonlinear Optics* (Wiley, 1984), Chap. 6, pp. 67–85.
13. M. M. Fejer, G. A. Magel, D. H. Jundt, and R. L. Byer, "Quasi-phase-matched second harmonic generation: tuning and tolerances," IEEE J. Quantum Electron. **28**, 2631–2654 (1992).
14. J. A. Armstrong, N. Bloembergen, J. Ducuing, and P. S. Pershan, "Interactions between light waves in a nonlinear dielectric," Phys. Rev. **127**, 1918–1939 (1962).
15. K. R. Parameswaran, J. R. Kurz, R. V. Roussev, and M. M. Fejer, "Observation of 99% pump depletion in single-pass second-harmonic generation in a periodically poled lithium niobate waveguide," Opt. Lett. **27**, 43–45 (2002).
16. R. L. Byer, "Optical parametric oscillators," in *Quantum Electronics: A Treatise, vol. I, Nonlinear Optics, Part B*, H. Rabin and C. L. Tang, eds. (Academic Press, 1975), pp. 587–702.
17. J. S. Pelc, P. S. Kuo, O. Slattery, L. Ma, X. Tang, and M. M. Fejer, "Dual-channel, single-photon upconversion detector at 1.3 μm," Opt. Express **20**, 19075–19087 (2012).
18. P. A. Jansson, *Deconvolution: with applications in spectroscopy* (Academic Press, 1984).
19. J. S. Pelc, C. Langrock, Q. Zhang, and M. M. Fejer, "Influence of domain disorder on parametric noise in quasi-phase-matched quantum frequency converters," Opt. Lett. **35**, 2804–2806 (2010).
20. M. H. Chou, J. Hauden, M. A. Arbore, and M. M. Fejer, "1.5-μm-band wavelength conversion based on difference-frequency generation in LiNbO$_3$ waveguides with integrated coupling structures," Opt. Lett. **23**, 1004–1006 (1998).
21. R. V. Roussev, "Optical-frequency mixers in periodically poled lithium niobate: materials, modeling and characterization," Ph.D. thesis, Stanford University (2006).
22. P. Kumar, "Quantum frequency conversion," Opt. Lett. **15**, 1476–1478 (1990).

1. Introduction

Upconversion detectors are useful for single-photon counting of telecommunications-band photons near 1.3 μm and 1.55 μm wavelengths [1–3] and for near-infrared spectroscopy [4,5]. This detection method is an attractive alternative to direct detection by InGaAs/InP avalanche photodiodes (APDs) that use gating to reduce after-pulsing and dark counts [6, 7], and superconducting single-photon detectors that require cryogenic cooling [6, 8]. Upconversion detection utilizes highly efficient sum-frequency generation (SFG), where signal photons at wavelength λ_s mix with a strong pump beam at λ_p to produce shorter-wavelength, sum-frequency (SF) photons at λ_{SF} that can then by detected by efficient detectors like silicon APDs. High-conversion SFG is typically achieved in long, nonlinear optical devices (such as periodically poled LiNbO$_3$ (PPLN) waveguides [2,9]) that inherently have narrow spectral acceptance bandwidths due to their lengths. By sweeping the pump wavelength, the signal acceptance band is tuned so that the upconversion detector acts as a spectrometer. An upconversion spectrometer for detection of 1.3 μm wavelengths was shown to have -126 dB sensitivity, which is several orders of magnitude better than traditional optical spectrum analyzers [5]. Even better sensitivity has been recently shown in an upconversion spectrometer [10]. Furthermore, this high sensitivity can be achieved under room-temperature operation without special cooling of the detector.

The spectral selectivity of the upconversion spectrometer is limited by the spectral acceptance bandwidth for the SFG process. For a 5 cm long PPLN waveguide, the spectral acceptance bandwidth is about 0.2 nm (full-width half maximum, FWHM) near 1310 nm or about 40 GHz [5, 11]. The actual spectral response of the waveguide is not a simple gate function but is more complicated, with a central peak and side lobes. In the low-conversion limit, the ideal spectral response function has a $\mathrm{sinc}^2[a(\lambda - \lambda_0)]$ shape, where $\mathrm{sinc}(x) = \sin(x)/x$ [5, 12, 13]. However, as the pump power is increased and photons at the signal wavelength become depleted, the spectral response function changes [14, 15]. It is desirable to work at the point of maximum conversion in order to obtain the highest system detection efficiency, but at this point, the spectral response of the upconversion device is different than its low-pump-power response. In this paper, we experimentally and theoretically investigate the spectral response

of an upconversion spectrometer as a function of pump power. At maximum conversion, the side lobes adjacent to the central peak are 2.5 times higher and the central peak is 0.9 times as narrow compared to the spectral response at very low pump power.

2. Theory

In sum-frequency generation, the SF, pump, and signal frequencies are related by $\omega_{SF} = \omega_p + \omega_s$. The electric fields in the upconversion waveguide are well-described by plane waves: $\mathscr{E}_i(z) = E_i(z) \sin(k_i z - \omega_i t)$ where E_i is the slowly varying field envelope, and k_i is the wavevector at frequency ω_i. Neglecting loss, the coupled wave equations for SFG are [16]

$$\frac{dE_p}{dz} = i\kappa_p E_{SF} E_s^* e^{i\Delta k z} \tag{1}$$

$$\frac{dE_s}{dz} = i\kappa_s E_{SF} E_p^* e^{i\Delta k z}$$

$$\frac{dE_{SF}}{dz} = i\kappa_{SF} E_p E_s e^{-i\Delta k z},$$

where $\kappa_i = \omega_i d_{\text{eff}}/n_i c$, $\Delta k = k_{SF} - k_p - k_s - 2\pi/\Lambda_G$, Λ_G is the quasi-phasematching [13] grating period, d_{eff} is the effective nonlinear coefficient, n_i is the refractive index at ω_i, and c is the speed of light. In SFG, the strong pump remains undepleted while the signal photons are converted to SF photons. If we assume $E_{SF}(0) = 0$ and $E_p(0) \gg E_s(0)$, the SF photon conversion efficiency in a crystal of length L is (see Appendix for a derivation [14])

$$\eta = \frac{N_{SF}(L)}{N_s(0)} = \frac{1}{1 + (\Delta k/2\Gamma)^2} \sin^2 \left(\Gamma L \sqrt{1 + (\Delta k/2\Gamma)^2} \right), \tag{2}$$

where N_i is the photon number and

$$\Gamma = \frac{d_{\text{eff}}}{c} \sqrt{\frac{2\omega_s \omega_{SF} I_p}{n_p n_s n_{SF} \varepsilon_0 c}}. \tag{3}$$

ε_0 is the permittivity of free space and $I_i = n_i \varepsilon_0 c |E_i|^2/2$ is the intensity at ω_i. In the low-conversion limit where $\Delta k/2\Gamma \gg 1$, Eq. (2) reduces to $\eta \propto \text{sinc}^2(\Delta k L/2)$. Also, at perfect phasematching ($\Delta k = 0$), Eq. (2) becomes

$$\eta = \sin^2(\Gamma L) = \sin^2 \left(\frac{\pi}{2} \sqrt{\frac{P_p}{P_{max}}} \right). \tag{4}$$

P_p is the pump power, which is the pump intensity integrated over area. Eq. (4) defines P_{max} as the pump power where maximum conversion is achieved.

3. Spectral distortion effects

Using Eq. (2), we calculated the theoretical spectral response functions for different pump powers. Figure 1 plots the effect of increasing pump power on the spectral response for an ideal upconversion waveguide. Figure 1(a) shows several tuning-curve shapes at different pumping powers, while Fig. 1(b) compares the spectra at $P_p/P_{max} = 0.25$ and 1 to a $\text{sinc}^2(\Delta k L/2)$ tuning curve. The dependence of the ratio of side-lobe to central-peak heights is shown in Fig. 1(c), and the central peak width is plotted in Fig. 1(d). For $P_p = P_{max}/4$, η is half of the maximum value and the spectral response already exhibits some small deviations from the $\text{sinc}^2(\Delta k L/2)$ function. As the pump power is increased, the heights of the side lobes increase relative to
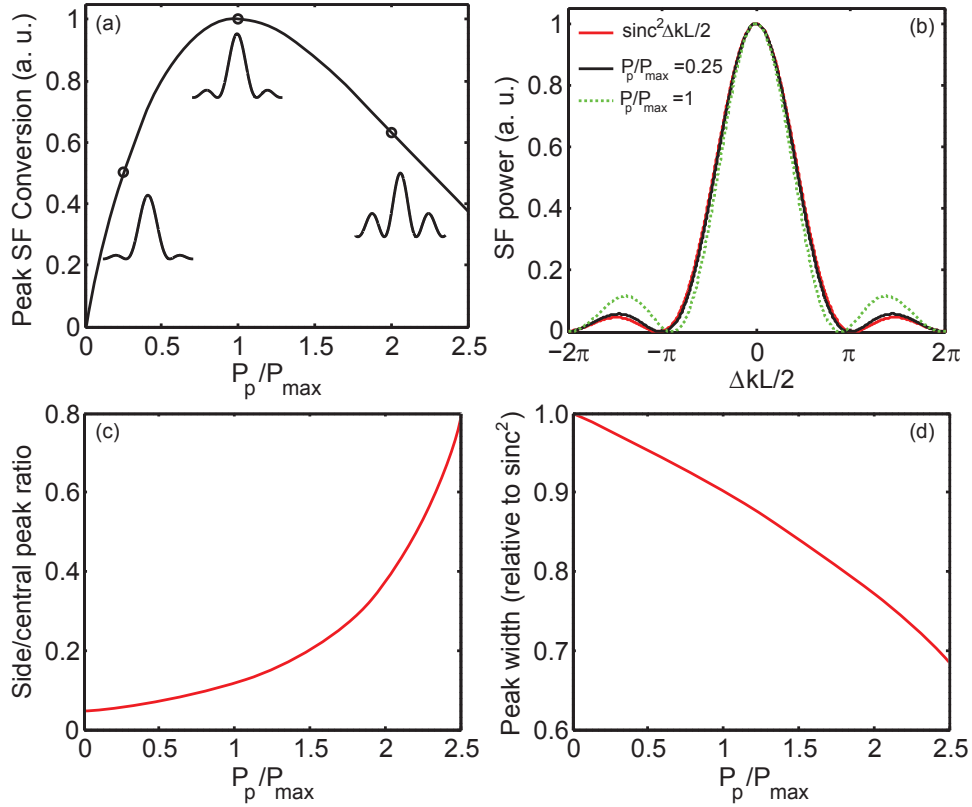
Fig. 1. (a) Theoretical SF conversion efficiency (in arbitrary units (a. u.)) and SF tuning curves at pump powers $P_p/P_{max} = 0.25$, 1, and 2. (b) Comparison of SF spectral tuning curves at $P_p/P_{max} = 0.25$ and 1, and a $\mathrm{sinc}^2(\Delta kL/2)$ tuning curve. (c) Calculated ratio of side-lobe height to central-peak height and (d) width of central peak (FWHM) for different pumping powers relative to FWHM of $\mathrm{sinc}^2(\Delta kL/2)$ function.

the central peak. In fact, the side lobes become equal in height to the central peak at $P_p/P_{max} = 2.645$. Also, the width of the central peak decreases and the side lobes move closer to the central peak for stronger pumping.

In an upconversion spectrometer, one would like to operate at maximum conversion ($P_p = P_{max}$) in order to get highest detection efficiency, but the spectral response of the device will have changed compared to its lower-power response. This change in shape is easiest to notice in the heights of the side lobes compared to the central peak. For an ideal $\mathrm{sinc}^2(\Delta kL/2)$ tuning curve (obtained at very low pump powers in an ideal waveguide), the side lobes are 4.7% the height of the main peak. From Fig. 1(c), at P_{max} the side lobes are 12% of the central peak height. That is, the side lobes are 2.5 times higher at P_{max} compared to the heights at very low pump power. If the device is pumped too hard ($P_p > P_{max}$), the SF conversion efficiency is diminished and the spectral response function is further distorted with even higher side lobes.

4. Experiment

We characterized the spectral response of an upconversion waveguide using the experimental setup in Fig. 2. SFG was performed in a reverse-proton exchanged PPLN waveguide [2, 9, 17] with 52 mm length, 13.5 μm period, and 50°C temperature. The waveguide input was
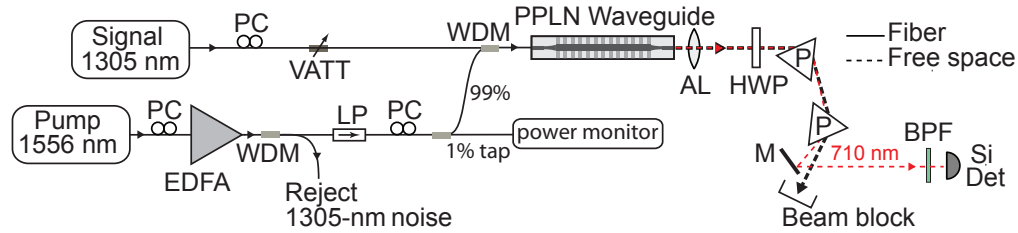
Fig. 2. Experimental setup. Sum frequency mixing of 1305 nm and 1556 nm beams to produce 709.7 nm SF photons is performed in a PPLN waveguide. The output of the waveguide is sent to two prisms at Brewster's angle that separate out the pump and signal beams. PC, polarization controller; VATT, variable attenuator; LP, linear polarizer; AL, aspheric lens; P, prism; M, mirror; BPF, bandpass filter; Si Det, silicon detector.

fiber-pigtailed and the free-space output was anti-reflection (AR) coated for all wavelengths of interest. The signal beam at 1305 nm from a continuous-wave (CW) laser was attenuated to 2 μW and combined with the pump beam at 1556 nm using a wavelength-division multiplexer (WDM). The pump was amplified in an erbium-doped fiber amplifier (EDFA) and filtered by three WDMs in series that rejected amplified spontaneous emission from the EDFA near 1300-nm wavelength. The output of the EDFA was passed through an inline polarizer to make sure the polarization state of the pump remained fixed. A 1% tap coupler and Ge detector followed the inline polarizer to monitor the pump power. The SF photons at 709.7 nm were collected by an AR-coated aspheric lens and directed to a pair of prisms that separated the SF photons from the pump and signal. Since the PPLN waveguide produced vertically polarized photons, a half-wave plate (HWP) was used to rotate the SF polarization into the plane of the experiment in order send p-polarized light to the uncoated prisms and obtain low loss at Brewster's angle. To characterize the tuning curves, we detected the 709.7 nm photons with a biased silicon detector preceded by a 20 nm bandpass filter to reject the 778 nm second harmonic of the pump.

We measured the conversion-efficiency spectra for different pump powers. The signal wavelength was fixed to 1305 nm while the pump wavelength was swept around 1556 nm. Figure 3(a) plots the maximum sum-frequency conversion for different pump powers. The pump powers are given at the fiber-pigtail input. Red circles are data while the black line is the fit to Eq. (4), which gives $P_{max} = 150$ mW. This point corresponds to total-system photon detection efficiency of 34% [11]. Figure 3(b) shows eight measured SF conversion spectra, which correspond to the eight red circles in Fig. 3(a). The spectra are normalized to the maximum value and are labeled by P_p/P_{max}.

As the pump power is increased, the heights of the side lobes rise. From the measured tuning curves, we examined the side lobes immediately to the left and right of the central peak, estimated their average height and divided this average by the central peak height to compute the side-to-central-peak height ratio. Figure 3(c) plots this measured ratio and compares it to the theoretical ratio for an ideal waveguide having $P_{max} = 150$ mW. In Fig. 3(d), the measured width of the central peak is compared to the theoretically predicted width. The theoretical width was calculated using $P_{max} = 150$ mW and low-power width equal to the measured width at 5 mW pump power. There is very good agreement between theory and experiment in both the side-to-central-peak ratio and central-peak width. The measured spectra show a slight shift of the peak wavelength as the pump power is increased, which may be due to drift in the temperature controller.
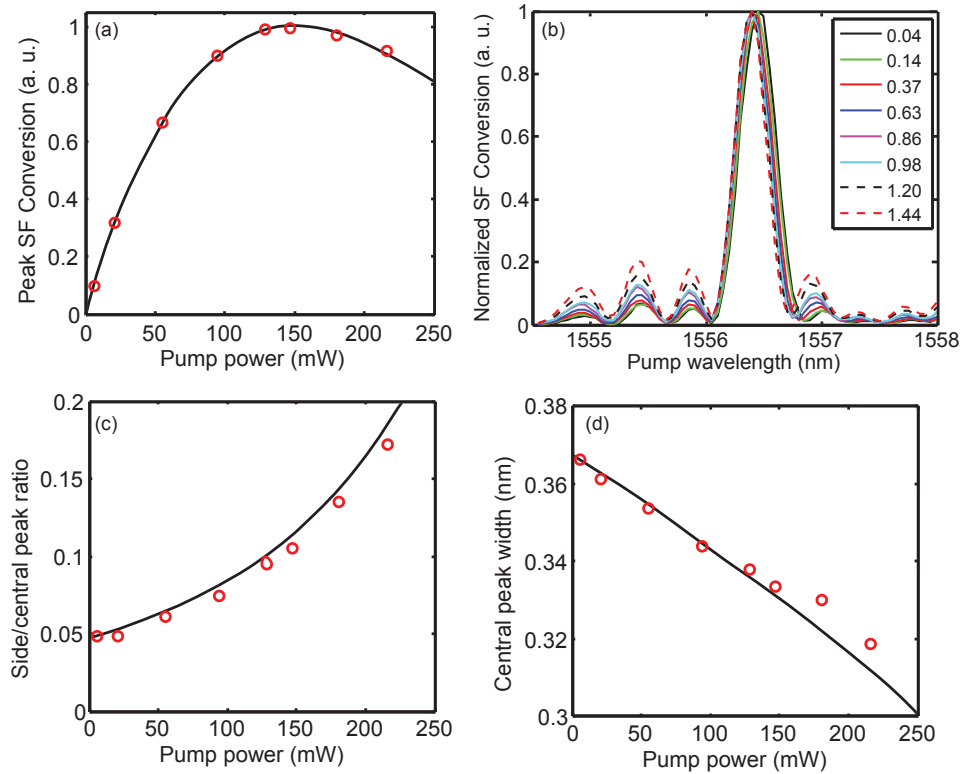
Fig. 3. (a) Measured peak conversion efficiency (red circles) and theoretical fit (black line). (b) Normalized sum-frequency conversion for different pump powers. Curves are labeled by P_p/P_{max} and correspond to red circles in (a). (c) Measured and theoretical ratio between side-lobe and central-peak heights. (d) Measured and theoretical full-width half maximum of the central peak.

5. Discussion

In an upconversion spectrometer, the apparent measured spectrum is a convolution of the actual spectrum and the SFG spectral response function [5, 10]. In practice, one should calibrate the upconversion spectrometer by characterizing its response to a δ-function (narrowband spectral) input, and use this measured function together with deconvolution algorithms [18] to extract the actual spectra from the raw, measured spectra. The work here shows that it is important to perform the spectral calibration measurement at the same pump power as the actual spectral measurements. For pump powers $P_p < P_{max}/4$, the SFG spectral response function is relatively constant, but for stronger pumps, the response changes noticably with pumping power. The scaling behavior decribed here can be applied to practical upconversion devices that may have non-ideal spectral response functions due to fabrication imperfections. For instance, the heights of the side lobes are 2.5 times higher when pumping for maximum conversion than they are at very low pump powers. Also, the smaller slopes at small P_p in Figs. 1(c) and 1(d) indicate that the spectra are less sensitive to variations in P_p for lower pumping than at higher pumping, which leads to better repeatibility of measurements.

Working at lower pump powers means that the system detection efficiency is lower. However, lower pump powers may be beneficial because they result in smaller dark count rates and improved signal-to-noise ratio (SNR) [11]. For detecting single-photon-level 1.3-μm wavelength

photons using prism filtering, we showed that the highest SNR was obtained at $P_p/P_{max} = 0.08$ [11]. Narrow spectral filtering of the upconverted beam reduces dark count rates and improves SNR. Noise photons are typically from spontaneous Raman scattering or spontaneous parametric downconversion and tend to be broadband compared to the signal [9, 19], so narrower filtering rejects more noise photons. In addition to reducing dark count rates, the narrower filtering raised the pump power where SNR was maximized, but this power was still below P_{max} [11]. We conclude that it is desirable to operate an upconversion detector at pump powers below P_{max} for improved signal-to-noise ratio and less distortion in the SFG spectral response function.

The measurement of the SFG spectral response may be done at μW-level signal powers where the SFG can be easily detected with standard photodiodes. Using the exact SFG solutions (see Appendix), we found that the spectral response was constant with respect to signal power so long as the photon numbers of the pump and signal satisfy $N_s < N_p/10$. However, raising the signal power too high can produce large SF powers at 710-nm wavelength inside the waveguide, which may induce photorefractive effects that can displace or cause instability in the spectrum [20, 21].

6. Conclusion

In this paper, we characterize the spectral response function for an upconversion spectrometer and show that the spectral response changes with the pump power. We derive analytic expressions for the spectral response for an ideal waveguide and show how the spectra evolve by growth of the side lobes and narrowing of the spectra. The response function remain fairly constant for $P_p < P_{max}/4$, but the side lobes become noticably higher for larger pump powers. At $P_p = P_{max}$, the side lobes are 2.5 times higher than the sizes at very low pump powers. Operating an upconversion spectrometer below maximum conversion may be attractive since the signal-to-noise ratio is better and the spectral response is less distorted. When using an upconversion spectrometer, a reference response spectrum should be characterized using a narrowband signal and used to deconvolve the true signal spectrum from a measured test spectrum. The reference spectral response should be measured at the same pump power as the test spectra. The evolving spectral response functions explored here are important to consider for upconversion detection and quantum frequency conversion [22], especially when the signal photons to be upconverted have non-negligible bandwidth, such as those produced from modelocked pulses or spontaneous parametric downconversion. The different spectral response functions are associated with different signal acceptance bandwidths, which also affect upconversion noise and dark count rates.

Appendix. Sum-frequency generation with high conversion efficiency

In this Appendix, we review the exact solutions for plane-wave, sum-frequency generation [12, 14] and derive the theoretical spectral response given in Eq. (2). Based on the slowly varying, electric field envelopes E_i, we define u_i and ϕ_i according to

$$u_i e^{-i\phi_i} = \sqrt{\frac{n_i c \varepsilon_0}{2\omega_i W}} E_i, \tag{5}$$

where the constant $W = I_p + I_s + I_{SF}$ is the total intensity. u_i^2 is proportional to the photon number and can be written as $u_i^2 = I_i/\omega_i W$. Conservation of total power means that $\omega_p u_p^2 + \omega_s u_s^2 + \omega_{SF} u_{SF}^2 = 1$.

Using these quantities, the coupled-wave equations (Eq. (1)) become

$$\frac{du_p}{dz} = -\Gamma' u_{SF} u_s \sin\theta \tag{6}$$

$$\frac{du_s}{dz} = -\Gamma' u_{SF} u_p \sin\theta$$

$$\frac{du_{SF}}{dz} = \Gamma' u_p u_s \sin\theta$$

$$\frac{d\theta}{dz} = \Delta k + \Gamma' \cos\theta \left(\frac{u_p u_s}{u_{SF}} - \frac{u_{SF} u_p}{u_s} - \frac{u_s u_{SF}}{u_p} \right),$$

where

$$\theta = \Delta k z + \phi_{SF} - \phi_p - \phi_s \tag{7}$$

and

$$\Gamma' = \frac{d_{\text{eff}}}{c} \sqrt{\frac{2\omega_p \omega_s \omega_{SF} W}{n_p n_s n_{SF} \varepsilon_0 c}}. \tag{8}$$

By substituting the first three expressions into the last equation of Eq. (6), and introducing $\zeta = \Gamma' z$ and $\Delta S = \Delta k/\Gamma'$, Eq. (6) becomes

$$\frac{du_p}{d\zeta} = -u_{SF} u_s \sin\theta \tag{9}$$

$$\frac{du_s}{d\zeta} = -u_{SF} u_p \sin\theta$$

$$\frac{du_{SF}}{d\zeta} = u_p u_s \sin\theta$$

$$\frac{d\theta}{d\zeta} = \Delta S + \cot\theta \frac{d}{d\zeta} \left[\ln(u_p u_s u_{SF}) \right].$$

The Manley-Rowe relations for photon-number conservation result in three constants [12, 14]

$$m_p = u_s^2 + u_{SF}^2 \tag{10}$$

$$m_s = u_p^2 + u_{SF}^2$$

$$m_{SF} = u_p^2 - u_s^2.$$

Equation (9) may be solved by first integrating the last equation to obtain

$$\cos\theta = (C_0 + \Delta S u_{SF}^2/2)/(u_p u_s u_{SF}), \tag{11}$$

where C_0 is a constant independent of ζ, and using this result to eliminate $\sin\theta$ to find

$$\frac{du_{SF}^2}{d\zeta} = \pm 2 \left[(u_p u_s u_{SF})^2 - (C_0 + \Delta S u_{SF}^2/2)^2 \right]^{1/2} \tag{12}$$

$$= \pm 2 \left[u_{SF}^2 (m_s - u_{SF}^2)(m_p - u_{SF}^2) - (C_0 + \Delta S u_{SF}^2/2)^2 \right]^{1/2}.$$

Rearranging Eq. (12) and integrating yields

$$\zeta = \pm \frac{1}{2} \int_{u_{SF}^2(0)}^{u_{SF}^2(\zeta)} \frac{d(u_{SF}^2)}{\left[u_{SF}^2 (m_s - u_{SF}^2)(m_p - u_{SF}^2) - (C_0 + \Delta S u_{SF}^2/2)^2 \right]^{1/2}}. \tag{13}$$

In [14], the solutions for u_{SF}^2 to the equation

$$u_{SF}^2(m_s - u_{SF}^2)(m_p - u_{SF}^2) - (C_0 + \Delta S u_{SF}^2/2)^2 = 0, \tag{14}$$

are introduced, and the three solutions are labeled by $u_{SF,c}^2 \geq u_{SF,b}^2 \geq u_{SF,a}^2 \geq 0$. The general solution to Eq. (13) is [14]

$$u_{SF}^2(\zeta) = u_{SF,a}^2 + (u_{SF,b}^2 - u_{SF,a}^2)\mathrm{sn}^2[(u_{SF,c}^2 - u_{SF,a}^2)^{1/2}(\zeta + \zeta_0), \gamma], \tag{15}$$

where sn is a Jacobi elliptic function, and the parameter γ is

$$\gamma = \sqrt{\frac{u_{SF,b}^2 - u_{SF,a}^2}{u_{SF,c}^2 - u_{SF,a}^2}}. \tag{16}$$

$u_p^2(\zeta)$ and $u_s^2(\zeta)$ are found by combining Eqs. (15) and (10).

The initial condition for sum-frequency generation is $u_{SF}(0) = 0$, which means that

$$
\begin{aligned}
m_p &= u_s^2(0) \\
m_s &= u_p^2(0) \\
C_0 &= 0.
\end{aligned}
\tag{17}
$$

$C_0 = 0$ implies $u_{SF,a}^2(0) = 0$, and the other two roots to Eq. (14) are

$$u_{SF,b}^2 = \frac{1}{2}\left(m_p + m_s + (\Delta S)^2/4 - \sqrt{(m_p + m_s + (\Delta S)^2/4)^2 - 4m_s m_p}\right) \tag{18}$$

$$u_{SF,c}^2 = \frac{1}{2}\left(m_p + m_s + (\Delta S)^2/4 + \sqrt{(m_p + m_s + (\Delta S)^2/4)^2 - 4m_s m_p}\right).$$

If we further assume that the pump is much stronger than the signal ($u_p^2(0) \gg u_s^2(0)$ and $m_s \gg m_p$), then

$$u_{SF,b}^2 = \frac{m_p m_s}{m_s + (\Delta S)^2/4} \tag{19}$$

$$u_{SF,c}^2 = m_s + (\Delta S)^2/4,$$

and

$$\gamma = \sqrt{u_{SF,b}^2/u_{SF,c}^2} = \frac{m_p m_s}{(m_s + (\Delta S)^2/4)^2} \approx 0. \tag{20}$$

Substituting these expressions into the solution Eq. (15) yields

$$u_{SF}^2(\zeta) = \frac{u_p^2(0)u_s^2(0)}{u_p^2(0) + (\Delta S)^2/4}\sin^2\left(\zeta\sqrt{u_p^2(0) + (\Delta S)^2/4}\right) \tag{21}$$

since $\mathrm{sn}(x, \gamma = 0) = \sin(x)$. If $u_p^2(0) \gg u_s^2(0)$ and $u_{SF}(0) = 0$, then $W = I_p(0)$, $u_p^2(0) = 1/\omega_p$, and $\Gamma' u_p(0) = \Gamma$ defined in Eq. (3). u_i^2 is proportional to photon number N_i, so that after converting back to physical parameters, we obtain

$$
\begin{aligned}
\frac{u_{SF}^2(\zeta = \Gamma' L)}{u_s^2(0)} &= \frac{N_{SF}(z = L)}{N_s(0)} \\
&= \frac{1}{1 + (\Delta k/2\Gamma)^2}\sin^2\left(\Gamma L\sqrt{1 + (\Delta k/2\Gamma)^2}\right).
\end{aligned}
\tag{22}
$$

Equation (22) holds under the assumption $u_p^2(0) \gg u_s^2(0)$, but the full solution can be found using $u_{SF,b}^2$ and $u_{SF,c}^2$ in Eq. (18). Numerically, we found that Eq. (22) was valid while $u_s^2(0)/u_p^2(0) < 0.1$.